PHYSICAL REVIEW B **87**, 115422 (2013)

New Dirac points and multiple Landau level crossings in biased trilayer graphene

Maksym Serbyn[1] and Dmitry A. Abanin[2,3,4]

[1]*Department of Physics, Massachusetts Institute of Technology, Cambridge, Massachusetts, USA*

[2]*Perimeter Institute for Theoretical Physical, Waterloo, Ontario, Canada*

[3]*Institute for Quantum Computing, Waterloo, Ontario, Canada*

[4]*Department of Physics, Harvard University, Cambridge, Massachusetts, USA*

(Received 15 January 2013; published 18 March 2013)

Recently a new high-mobility Dirac material, trilayer graphene, was realized experimentally. The band structure of ABA-stacked trilayer graphene consists of a monolayer-like and a bilayer-like pair of bands. Here we study electronic properties of ABA-stacked trilayer graphene biased by a perpendicular electric field. We find that the combination of the bias and trigonal warping gives rise to a set of new Dirac points: In each valley, seven species of Dirac fermions with small masses of order of a few meV emerge. The positions and masses of the emergent Dirac fermions are tunable by bias, and one group of Dirac fermions becomes massless at a certain bias value. Therefore, in contrast to bilayer graphene, the conductivity at the neutrality point is expected to show nonmonotonic behavior, becoming of the order of a few e^2/h when some Dirac masses vanish. Further, we analyze the evolution of the Landau level spectrum as a function of bias. The emergence of new Dirac points in the band structure translates into new threefold-degenerate groups of Landau levels. This leads to an anomalous quantum Hall effect, in which some quantum Hall steps have a height of $3e^2/h$. At an intermediate bias, the degeneracies of all Landau levels get lifted, and in this regime all quantum Hall plateaus are spaced by e^2/h. Finally, we show that the pattern of Landau level crossings is very sensitive to certain band structure parameters, and can therefore provide a useful tool for determining their precise values.

DOI: 10.1103/PhysRevB.87.115422 PACS number(s): 73.22.Pr, 72.80.Vp, 71.70.Di

I. INTRODUCTION

Single- and multiple-layer graphene materials are gapless 2D semimetals with unusual band structure, in which low-energy excitations have nontrivial Berry phases.[1] In particular, low-energy excitations in graphene are two species (valleys) of massless Dirac-like fermions with linear dispersion and Berry phase π. The excitations in bilayer graphene are chiral fermions with a parabolic dispersion relation and a Berry phase of 2π.[1] The unusual nature of excitations underlies fundamental phenomena found in these materials, including Klein tunneling, weak antilocalization, anomalous quantum Hall effects, as well as novel symmetry-broken states in high magnetic field.[1]

One important distinct feature of bilayer graphene (as compared to monolayer graphene and other 2D electron systems) is a unique tunability of its band structure. By applying a perpendicular electric field[2–4] which induces an asymmetry between the top and bottom layer, it is possible to induce a band gap of up to 250 meV.[4] Thus, bilayer graphene can be turned into a semiconductor with a widely tunable band gap, which makes it attractive for various device applications, and provides a way to study chiral carriers in new regimes.

Very recently, a new carbon-based semimetal, trilayer graphene, has been realized experimentally.[5–8] Experimentally studied trilayer graphene samples had a high mobility and exhibited the quantum Hall effect (QHE). Inspired by these experiments, in this paper we study the effect of a perpendicular electric field on the electronic properties of trilayer graphene. First, we aim to understand how the band structure of trilayer graphene transforms under bias, and to explore new possibilities offered by its tunability. Second, we would like to develop an understanding of Landau level (LL) evolution and LL crossings under bias. Given that the band structure of trilayer graphene is quite complicated, it is necessary to first understand single-particle effects in LL evolution, before addressing interaction phenomena, including quantum Hall ferromagnetism and fractional QHE.

Depending on the stacking (ABA or ABC), the band structure of trilayer graphene can be very different.[7,9–12] Throughout the paper, we will focus on the case of Bernal-stacked (ABA) trilayer graphene.[5,6] In the absence of bias, the band structure of ABA-trilayer graphene can be viewed as a combination of independent overlapping monolayer-like (Berry phase π) and bilayer-like bands (Berry phase 2π).[9,13–15] Both bands are gapped, in contrast to gapless monolayer and bilayer graphene; however, the monolayer-like and bilayer-like gaps are overlapping such that there is no band gap. In contrast, ABC-stacked trilayer graphene has Dirac points with cubic band touching and Berry phase 3π,[10,11] split by different symmetry-breaking terms.

Previously, it was noted that perpendicular electric field completely transforms the band structure of trilayer graphene, hybridizing the monolayer-like and bilayer-like bands,[9,16] and generally opening only a small band gap. Here we explore the transformation of the band structure in detail. Most interestingly, we find that as a result of trigonal warping, at bias $\sim$0.5 V/nm,[17] *seven* new Dirac points (DPs) emerge in each valley. One of the DPs is situated at the K_+ (K_-) point in the Brillouin zone; the remaining six consist of two groups of three, related to each other by $2\pi/3$ rotations. The emergent Dirac fermions are massive, with both their mass and velocity being tunable by an electric field. At electric field $\sim$0.9 V/nm,[17] the band gap closes for three DPs. For higher bias the mass of these DPs changes sign, and overall gap increases monotonically.

We analyze the evolution of LLs under bias, finding a very complex pattern of levels crossings and splittings. We illustrate the extreme sensitivity of this pattern with respect to band structure parameters. Even small variations of certain

 ©2013 American Physical Society

parameters change the pattern of crossings at small bias. Therefore, the Landau level crossings should provide a useful tool for precise determination of the band structure parameters, which are still a subject of debate.[5,18] The transformation of the band structure at high bias leads to an emergent threefold degeneracy of some Landau levels in magnetic field. It is worth noting that the evolution of LLs with bias has been previously discussed by McCann and Koshino in Ref. 13, who, however, considered an idealized model that neglected several smaller hopping parameters (see also Ref. 19). Here we consider the full tight-binding model,[5] finding that the smaller parameters play an important role in determining the pattern of LL crossings.

Our results also imply that single-particle physics in ABA trilayer graphene is much more complicated as compared to other chiral materials, such as monolayer and bilayer graphene, and it should be understood before addressing the interaction effects. On the positive side, the tunability of the band structure may prove advantageous in studying and tuning correlated states, including fractional quantum Hall states,[20,21] as discussed in the end of the paper.

The rest of the paper is organized as follows: In the next section we introduce the tight-binding description for the ABA-stacked trilayer graphene and review decoupling of its band structure into monolayer-like and bilayer-like blocks.[9] In Sec. III we discuss the evolution of the band structure as a function of perpendicular electric field. The Landau level spectrum as a function of magnetic field and electric field is studied in Sec. IV. Finally, in Sec. V, we provide a brief summary of our results and present a broader outlook.

II. MODEL AND REVIEW OF UNBIASED CASE

In this section, we introduce the tight-binding model of the ABA-stacked trilayer graphene and briefly review the derivation of low-energy effective Hamiltonian in the absence of bias following Ref. 9. We will discuss that in the absence of the perpendicular electric field (also referred to as the displacement field), the band structure can be viewed as two independent bands: one bilayer-graphene-like and the other monolayer-graphene-like.[9,13–15]

A. Tight-binding model

In order to describe the band structure of the unbiased trilayer graphene, we adopt the standard Slonczewski-Weiss-McClure parametrization of the tight-binding model.[18] Corresponding tight-binding parameters are schematically illustrated in Fig. 1. Six tight-binding parameters $\gamma_0 \dots \gamma_5$ describe hopping matrix elements between different atoms:

$$A_i \leftrightarrow B_i : \gamma_0, \quad B_{1,3} \leftrightarrow A_2 : \gamma_1, \tag{1a}$$

$$A_1 \leftrightarrow A_3 : \tfrac{1}{2}\gamma_2, \quad A_{1,3} \leftrightarrow B_2 : \gamma_3, \tag{1b}$$

$$\begin{matrix} A_{1,3} \leftrightarrow A_2 \\ B_{1,3} \leftrightarrow B_2 \end{matrix} : -\gamma_4, \quad B_1 \leftrightarrow B_3 : \tfrac{1}{2}\gamma_5, \tag{1c}$$

where A_i (B_i) refers to an atom from the A (B) sublattice, and index $i = 1 \dots 3$ labels three layers (see Fig. 1 for notation of sublattices). In addition, parameter δ accounts for an extra on-site potential for B_1, A_2, and B_3 sites, which are on top of each other. The values of different tight-binding parameters are far from being settled. In particular, the authors of Ref. 5 used experimentally determined higher LLs crossings to refine the values of tight-binding parameters. Corresponding values are listed in Fig. 1 and will be used in what follows.

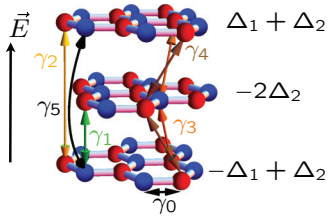

par.	value
γ_0	3.1 eV
γ_1	0.39 eV
γ_2	-0.028 eV
γ_3	0.315 eV
γ_4	0.041 eV
γ_5	0.05 eV
δ	0.046 eV

FIG. 1. (Color online) Schematic view of the lattice structure of the ABA-stacked trilayer graphene (left) and values of corresponding tight-binding parameters adopted from Ref. 5 (right). Red (blue) atoms belong to A (B) sublattice of the corresponding layer. Next to each layer, the potential energy of electrons expressed via parameters Δ_1 and Δ_2 is shown.

The effect of an external perpendicular electric field (displacement field) can be described by including additional on-site potentials for different layers $U_1 \dots U_3$.[9,22–24] It is convenient to introduce parameters

$$\Delta_1 = (-e)\frac{U_1 - U_2}{2}, \qquad \Delta_2 = (-e)\frac{U_1 - 2U_2 + U_3}{6}. \tag{2}$$

Physically, parameter Δ_1 is responsible for the potential difference between top and bottom layers which is caused by the application of the displacement field to the sample. Parameter Δ_2 describes the deviation of potential on the middle layer from the mean of the potentials on the top and bottom layers. As we shall discuss below, nonzero parameter Δ_2 can emerge when screening is taken into account and the potential distribution is calculated self-consistently. In principle, even *without bias*, a nonzero value of Δ_2 is allowed by symmetry. In what follows we will demonstrate that the LL crossing pattern is very sensitive to precise value of Δ_2.

For our analysis below, it will be convenient to separate the Hamiltonian of the unbiased trilayer, H_0, from terms related to the potential imbalance between layers,

$$H = H_0 + H_{\Delta_1} + H_{\Delta_2}. \tag{3}$$

In the momentum representation, the tight-binding Hamiltonian can be written in a compact matrix form, with different components corresponding to the wave function amplitudes on the six sublattices. Let us choose the basis $\{A_1, B_1, A_2, B_2, A_3, B_3\}$. In this basis, the three terms in the Hamiltonian can be written as

$$H_0 = \begin{pmatrix} 0 & \gamma_0 t_{\boldsymbol{k}}^* & \gamma_4 t_{\boldsymbol{k}}^* & \gamma_3 t_{\boldsymbol{k}} & \gamma_2/2 & 0 \\ \gamma_0 t_{\boldsymbol{k}} & \delta & \gamma_1 & \gamma_4 t_{\boldsymbol{k}}^* & 0 & \gamma_5/2 \\ \gamma_4 t_{\boldsymbol{k}} & \gamma_1 & \delta & \gamma_0 t_{\boldsymbol{k}}^* & \gamma_4 t_{\boldsymbol{k}} & \gamma_1 \\ \gamma_3 t_{\boldsymbol{k}}^* & \gamma_4 t_{\boldsymbol{k}} & \gamma_0 t_{\boldsymbol{k}} & 0 & \gamma_3 t_{\boldsymbol{k}}^* & \gamma_4 t_{\boldsymbol{k}} \\ \gamma_2/2 & 0 & \gamma_4 t_{\boldsymbol{k}}^* & \gamma_3 t_{\boldsymbol{k}} & 0 & \gamma_0 t_{\boldsymbol{k}}^* \\ 0 & \gamma_5/2 & \gamma_1 & \gamma_4 t_{\boldsymbol{k}}^* & \gamma_0 t_{\boldsymbol{k}} & \delta \end{pmatrix}, \tag{4}$$

$$H_{\Delta_1} = \mathrm{diag}(\Delta_1, \Delta_1, 0, 0, -\Delta_1, -\Delta_1), \tag{5}$$

$$H_{\Delta_2} = \mathrm{diag}(\Delta_2, \Delta_2, -2\Delta_2, -2\Delta_2, \Delta_2, \Delta_2). \tag{6}$$

In Eq. (4) we used $t_{\boldsymbol{k}}$ as a short-hand notation for a sum over nearest neighbors in a single honeycomb lattice:

$$t_{\boldsymbol{k}} = \sum_{j=1}^{3} e^{i\boldsymbol{k}\cdot\boldsymbol{a}_j} = -1 - 2e^{\sqrt{3}ik_y/2}\cos\frac{k_x}{2}, \tag{7}$$

where $\boldsymbol{a}_1 = (0, 1/\sqrt{3})$, $\boldsymbol{a}_{2,3} = (\mp 1/2, -1/2\sqrt{3})$, are vectors connecting an A_1 site to its nearest neighbors, and momenta are measured in units of inverse lattice constant, $a = 2.46$ Å.

To obtain an effective low-energy Hamiltonian, we expand Eq. (4) in the vicinity of K_+ and K_- points, located at position $(\pm 4\pi/3, 0)$ in the hexagonal Brillouin zone. This expansion reduces to replacing $\gamma_i t_{\boldsymbol{k}} \to v_i \pi$, where

$$\pi = \xi k_x + i k_y, \quad \hbar v_i = \frac{\sqrt{3}}{2} a\gamma_i, \tag{8}$$

with $\xi = \pm 1$ for K_+ and K_- points, respectively.

B. Effective Hamiltonian of unbiased trilayer graphene

In the absence of external bias, the band structure of the Hamiltonian (3) consists of monolayer-like and bilayer-like bands, as shown by Koshino and McCann.[13] To illustrate the decoupling of the Hamiltonian, we consider a different basis,

$$\left\{\frac{A_1 - A_3}{\sqrt{2}}, \frac{B_1 - B_3}{\sqrt{2}}, \frac{A_1 + A_3}{\sqrt{2}}, B_2, A_2, \frac{B_1 + B_3}{\sqrt{2}}\right\}. \tag{9}$$

In the new basis, the sum of two terms, $H_0 + H_{\Delta_2}$ (Δ_2 is allowed by symmetry even in the absence of electric field) acquires a block-diagonal structure,

$$H_0 + H_{\Delta_2} = \begin{pmatrix} H_{\rm SLG} & 0 \\ 0 & H_{\rm BLG} \end{pmatrix}, \tag{10}$$

where the monolayer-like and bilayer-like blocks are defined as

$$H_{\rm SLG} = \begin{pmatrix} \Delta_2 - \frac{\gamma_2}{2} & v_0\pi^\dagger \\ v_0\pi & -\frac{\gamma_5}{2} + \delta + \Delta_2 \end{pmatrix}, \tag{11a}$$

$$H_{\rm BLG} = \begin{pmatrix} \frac{\gamma_2}{2} + \Delta_2 & \sqrt{2}v_3\pi & -\sqrt{2}v_4\pi^\dagger & v_0\pi^\dagger \\ \sqrt{2}v_3\pi^\dagger & -2\Delta_2 & v_0\pi & -\sqrt{2}v_4\pi \\ -\sqrt{2}v_4\pi & v_0\pi^\dagger & \delta - 2\Delta_2 & \sqrt{2}\gamma_1 \\ v_0\pi & -\sqrt{2}v_4\pi^\dagger & \sqrt{2}\gamma_1 & \frac{\gamma_5}{2} + \delta + \Delta_2 \end{pmatrix}. \tag{11b}$$

The effective Hamiltonian of the bilayer-like sector can be simplified further by noting that the low-energy states predominantly reside on $A_1 + A_3$ and on B_2 sublattices. The higher energy bands, which reside mostly on sublattices $B_1 + B_3, A_2$ have a large band gap of order $\pm\sqrt{2}\gamma_1 \sim 0.5$ eV. Taking into account virtual excitations to these bands, one obtains an effective 2×2 Hamiltonian of the bilayer-like band:[25]

$$H_{\rm BLG} \approx H^{(0)}_{\rm BLG} + H^{(1)}_{\rm BLG}, \tag{12}$$

where $H^{(0)}_{\rm BLG}$ is the leading approximation,

$$H^{(0)}_{\rm BLG} = -\frac{1}{2m}\begin{pmatrix} 0 & \pi^{\dagger 2} \\ \pi^2 & 0 \end{pmatrix}, \quad \frac{1}{2m} = \frac{v^2}{\sqrt{2}\gamma_1}, \tag{13}$$

and $H^{(1)}_{\rm BLG}$ describes various corrections:

$$H^{(1)}_{\rm BLG} = \sqrt{2}v_3\begin{pmatrix} 0 & \pi \\ \pi^\dagger & 0 \end{pmatrix} + \begin{pmatrix} \gamma_2/2 + \Delta_2 & 0 \\ 0 & -2\Delta_2 \end{pmatrix} + \frac{v^2}{2\gamma_1}\begin{pmatrix} (\delta - 2\Delta_2)\pi^\dagger\pi & 0 \\ 0 & (\gamma_5/2 + \delta + \Delta_2)\pi\pi^\dagger \end{pmatrix}. \tag{14}$$

Note that in the above expression for $H^{(1)}_{\rm BLG}$ we omitted terms which renormalize mass in $H^{(0)}_{\rm BLG}$ [Eq. (13)]. Also, the last term in Eq. (14) does not include contributions which come with an additional small parameter $\gamma_1\gamma_4/(\gamma_0\delta) \approx 0.11$.

Therefore, in the limit when there is no electric field ($\Delta_1 = 0$), the band structure of ABA-stacked trilayer graphene has SLG and BLG sectors which are decoupled from each other. The resulting band structure of the unbiased trilayer is illustrated in Fig. 2(a).

When a displacement field is applied, the reflection symmetry between the top and bottom layer is broken and the H_{Δ_1} appears in the Hamiltonian (note that electric field also affects Δ_2, which, in general, should be calculated self-consistently; see below). In the rotated basis (9) this term corresponds to hybridization between the monolayer-like and bilayer-like blocks and has the form

$$H_{\Delta_1} = \begin{pmatrix} 0 & H_{\rm hyb} \\ H^T_{\rm hyb} & 0 \end{pmatrix}, \quad H_{\rm hyb} = \begin{pmatrix} \Delta_1 & 0 & 0 & 0 \\ 0 & 0 & 0 & \Delta_1 \end{pmatrix}. \tag{15}$$

As a next step, we will discuss the evolution of the bands resulting from this hybridization.

III. BAND STRUCTURE EVOLUTION UNDER BIAS: A NEW SET OF DIRAC POINTS

An electric field completely changes the low-energy properties of trilayer graphene, hybridizing the monolayer- and bilayer-like bands. In this section we shall study how the bands transform as bias increases. We will see that at relatively small bias, there is a complex interplay of terms induced by electric field and smaller trigonal warping terms in the Hamiltonian, which gives rise to rather flat low-energy bands. At higher bias ($\Delta_1 \gtrsim 0.1$ eV), a new set of Dirac points emerges: There are a total of seven DPs in each valley, one of them situated at $K_\pm$, and two groups of three related by rotational symmetry. The positions, mass gaps, as well as velocities of these DPs change as a function of bias.

Since analytical treatment is no longer possible, we resort to numerical diagonalization of the tight-binding Hamiltonian (4). The evolution of the band structure in valley K_+ as Δ_1 is changed from zero to 0.25 eV is illustrated in Fig. 2. Notice that the band structure in the K_- valley is related to that in the K_+ valley by the time-reversal symmetry. Throughout this section, we will put $\Delta_2 = 0$, because Δ_2 is expected to be of the order of several meV, and we find that it cannot qualitatively change the band structure. We emphasize, however, that Δ_2 will play an important role for the LL spectrum and LL crossing pattern in Sec. IV.

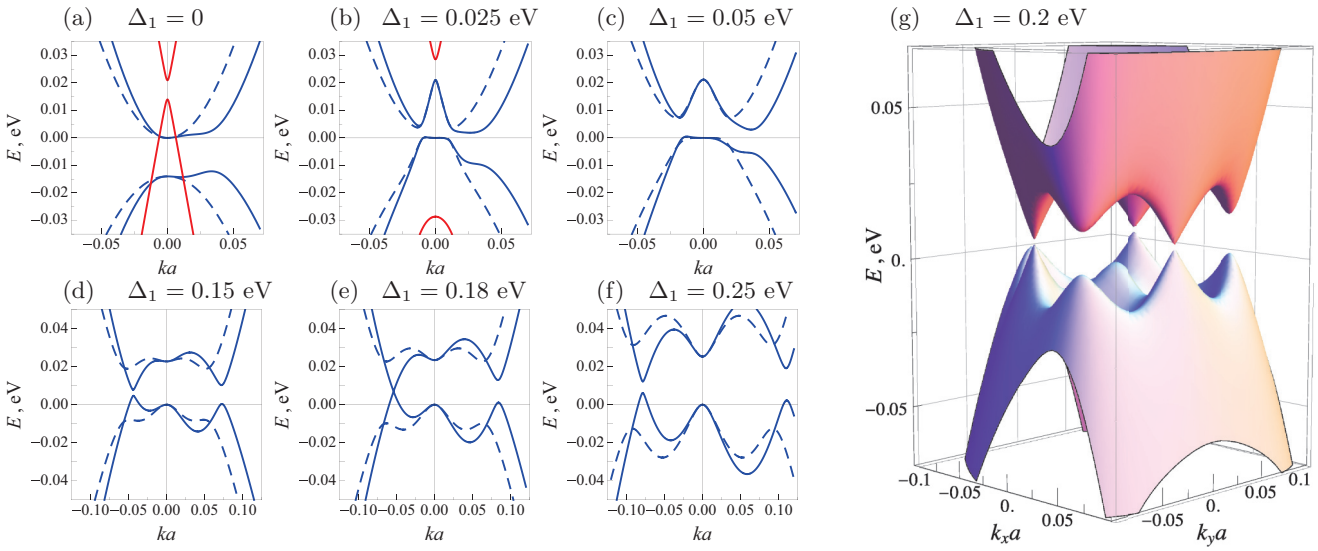

FIG. 2. (Color online) Evolution of the band structure of trilayer graphene with bias Δ_1. The bands in the vicinity of K_+ point in the Brillouin zone are shown as a function of ka, where $\boldsymbol{k}$ describes momentum relative to the K_+ point. Solid (dashed) lines correspond to $\boldsymbol{k}$ parallel to the x axis (y axis). At zero bias [panel (a)], red and blue lines describe monolayer-like and bilayer-like bands. At nonzero bias the monolayer-like and bilayer-like bands hybridize and no clear distinction can be made between them. As a result of this hybridization, one pair of bands moves to higher energies. The other pair of bands undergoes a series of transformations which lead to seven emergent Dirac points at higher bias $\Delta_1 \gtrsim 0.1$ meV. The positions of these Dirac points in the Brillouin zone are illustrated in panel (g).

The band structure in the absence of bias, Fig. 2(a), consists of a monolayer-like band (shown in red) and a trigonally warped bilayer-like band (shown in blue). Relatively small bias $\Delta_1 \approx 0.025$ eV in Fig. 2(b) turns out to be sufficient to hybridize bands; a electron-like and a hole-like band which used to be of monolayer type drift away to higher energies. The band gap for these bands becomes of the order 0.03 eV already at $\Delta_1 = 0.025$ eV, which means that they will be essentially irrelevant for the low-energy properties.

As the bias is increased further [$\Delta_1 = 0.05$ eV in Fig. 2(c)], the two remaining bands stay close to the neutrality point, and they are separated by a small band gap of the order of a few tens of meV. Near the K points, the bands have a complicated dispersion relation and trigonal warping is important. One notable feature is that the hole-like band is nearly flat in the vicinity of the K_+ point.

When Δ_1 becomes larger than 0.1 eV, the evolution of the bands leads to seven new Dirac points: one at the K_+ point, and six situated off-center. The off-center DPs consist of two groups of three, related by threefold rotational symmetry. All Dirac points are generally split by a small mass. The locations and splittings of the emergent DPs for $\Delta_1 = 0.2$ eV are illustrated in Fig. 2(g). In the interval of values $\Delta_1 =$ 0.15–0.25 eV, the off-center DPs move further away from the K_+ point. Also, for one of the groups the band gap closes and the Dirac mass changes sign at $\Delta_1 \approx 0.18$ eV [see Figs. 2(d)–2(g)]. The velocity also changes, although not very significantly.

To understand the origin of the new DPs and some of their properties, including their position in the Brillouin zone, let us reinspect the tight-binding model at large bias. We note that at large bias, the most important terms in the band structure are $\gamma_0, \gamma_1, \gamma_3$, and Δ_1. It is convenient to separate the Hamiltonian into the leading part which contains only these terms, $H^{(0)}$, and the remaining subleading part, $H^{(1)}$:

$$H = H^{(0)} + H^{(1)}. \tag{16}$$

To elucidate the structure of $H^{(0)}$ let us rearrange the basis (9) as follows:

$$\left\{ \frac{A_1 - A_3}{\sqrt{2}}, B_2, \frac{B_1 + B_3}{\sqrt{2}}, \frac{A_1 + A_3}{\sqrt{2}}, A_2, \frac{B_1 - B_3}{\sqrt{2}} \right\}. \tag{17}$$

Using Eqs. (4) and (5), we write $H^{(0)}$ in the vicinity of the K_+ point in the new basis:

$$H^{(0)} = \begin{pmatrix} 0 & C \\ C^\dagger & 0 \end{pmatrix}, \quad C = \begin{pmatrix} \Delta_1 & 0 & v_0\pi^\dagger \\ \sqrt{2}v_3\pi^\dagger & v_0\pi & 0 \\ v_0\pi & \sqrt{2}\gamma_1 & \Delta_1 \end{pmatrix}. \tag{18}$$

Similarly, one can find an explicit form of the subleading part of $H^{(1)}$, but we will not need it here.

The chiral symmetry of the Hamiltonian (18) greatly simplifies the analysis of its band structure. This symmetry implies that the spectrum is particle-hole symmetric. We find that for any Δ_1, $H^{(0)}$ has seven massless DPs. Their positions can be found from condition $\det C = 0$, which reduces to an algebraic equation on π:

$$\Delta_1^2 v_0\pi + v_0\pi^* \left(2\gamma_1 v_3 \pi^* - v_0^2 \pi^2\right) = 0. \tag{19}$$

First of all, $\pi = 0$ is an obvious root of the above equation. Second, introducing parametrization $\pi = pe^{i\theta}$, we obtain the other roots which give the positions of the remaining six

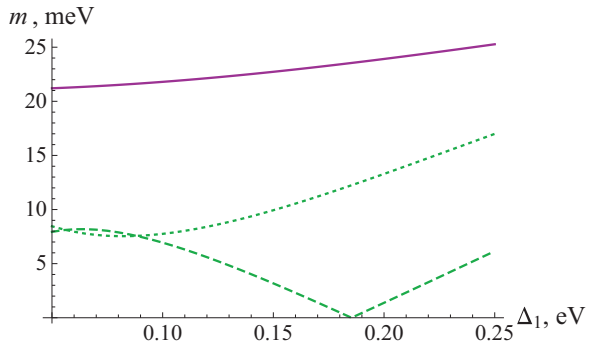

FIG. 3. (Color online) Evolution of the mass of emergent Dirac fermions as a function of bias $\Delta_1 = 0.05 \ldots 0.25$ eV for central DP (purple), first group of off-center DPs (dotted green), and second group of off-center DPs (dashed green). The mass of the second group of DPs vanishes at $\Delta_1 \approx 0.185$ eV and becomes negative at a larger bias.

off-center DPs:

$$p_1 = \frac{\sqrt{\gamma_1^2 v_3^2 + \Delta_1^2 v_0^2} + \gamma_1 v_3}{v_0^2}, \quad \theta = 0, 2\pi/3, 4\pi/3, \tag{20}$$

$$p_2 = \frac{\sqrt{\gamma_1^2 v_3^2 + \Delta_1^2 v_0^2} - \gamma_1 v_3}{v_0^2}, \quad \theta = \pi/3, \pi, 5\pi/3. \tag{21}$$

Therefore, at small $\Delta_1 \ll \gamma_1 v_3/v_0 \approx 0.04$ eV the off-center DPs remain relatively close to the K_+ point and their position depends approximately quadratically on Δ_1: $p_1 \approx 2\gamma_1 v_3/v_0^2 + \Delta_1^2/(2\gamma_1 v_3)$, $p_2 \approx \Delta_1^2/(2\gamma_1 v_3)$. At large bias, $\Delta_1 \gg 0.04$ eV, the distance of the off-center DPs from K_+ grows linearly with Δ_1, $p_{1(2)} \approx (\Delta_1 v_0 \pm \gamma_1 v_3)/v_0^2$.

The chiral symmetry is broken by the subleading part of the Hamiltonian, $H^{(1)}$ in Eq. (16). Consequently, all seven species of emergent Dirac fermions become massive, as is evident from Fig. 2. We extract the Dirac mass as a function of bias for these DPs from the numerically evaluated spectrum.[26] The result is illustrated in Fig. 3. The most interesting feature is that the mass of the second group of Dirac fermions vanishes at $\Delta_1^* \approx 0.185$ eV and changes sign for larger values of Δ_1. Note, that the value of Δ_1^* depends on the tight-binding parameters. The mass of the first group of Dirac fermions grows monotonically, changing from 8 meV at $\Delta_1 = 0.1$ eV to 18 meV at $\Delta_1 = 0.25$ eV. Finally, the mass of the central DP depends on bias relatively weakly.

The tunability of the Dirac masses will manifest itself in a characteristic nonmonotonic bias dependence of conductivity at the neutrality point. At $\Delta_1 < \Delta_1^*$ and $\Delta_1 > \Delta_1^*$ we expect an activated temperature dependence of the conductivity with an activation gap set by the smaller of the Dirac masses. When $\Delta_1 \approx \Delta_1^*$, assuming the disorder is weak, the conductivity will have a metallic temperature dependence and will be dominated by the twelve species of massless Dirac fermions (including spin and valley degeneracy), becoming of the order of $12 \times e^2/h$ (we assumed that a single Dirac species has a conductivity approximately equal to e^2/h[1]).

We note that as previously pointed out by McCann and Koshino,[9,27] the screening can be significant, and therefore the parameters Δ_1, Δ_2 should be calculated self-consistently. We have calculated the self-consistent values of Δ_1, Δ_2 as a function of external bias in the Hartree approximation, obtaining results which were consistent with Refs. 9, 27. Interestingly, there is nonzero $\Delta_2 \approx 2$ meV even at zero external bias. This term will be important in our analysis of low-lying LLs in the following section.

IV. LANDAU LEVELS AND THEIR CROSSINGS

In this section, we analyze the Landau level spectrum of the biased trilayer graphene. As we shall see, the bias-induced band structure transformations lead to a rich pattern of LL crossings. At high bias, when the new Dirac points are formed, corresponding threefold-degenerate groups of LLs emerge. This gives rise to an anomalous sequence of quantum Hall plateaus. At smaller bias, all LL degeneracies are lifted, and therefore all quantum Hall plateaus are spaced by e^2/h. An interesting feature of the LL crossing pattern is its extreme sensitivity to certain tight-binding parameters, including Δ_2 and γ_3. We explore how the existence and positions of various crossings depend on the values of these parameters, and argue that in an experiment the LL crossing pattern can be used to determine the precise values of tight-binding parameters.

A. Zero Landau levels without displacement field

We start with reviewing known results about the LL spectrum in the absence of bias.[13,19,28,29] In what follows, we shall be mostly interested in the low-lying LLs. The energies of such LLs in the unbiased case can be obtained analytically[28,29] from the effective low-energy model described in Sec. II A. This will facilitate the identification of various low-lying LLs in numerical simulations, and also will help us to develop an intuition about their sensitivity to tight-binding parameters.

In the absence of bias, the monolayer-like [Eq. (11a)] and bilayer-like [Eqs. (13) and (14)] bands are independent. To find the spectrum of LLs, we adopt the Landau gauge, $A_x = 0$, $A_y = Bx$, and make a substitution $\pi \to \pi - e(A_x + iA_y)$ in Eqs. (11a), (13), and (14). Momentum k_y is conserved (and is proportional to the guiding center position X), and the π operator acquires the following form ($\xi = \pm 1$ for $K_\pm$ valleys):

$$\pi = -\frac{i\hbar}{l_B}(\xi \partial_x + x - X), \tag{22}$$

where the coordinate and momentum are measured in units of magnetic length $l_B = \sqrt{\hbar/eB}$ and $1/l_B$, respectively. We see that π and $\pi^\dagger$ can be viewed as lowering and raising operators of the magnetic oscillator. In the basis of nonrelativistic LL orbitals $|n\rangle$ (at a given X), the matrix elements of $\pi, \pi^\dagger$ in the two valleys are given by

$$\begin{aligned} K_+ : \pi|n\rangle &= \frac{i\hbar}{l_B}\sqrt{2(n+1)}|n+1\rangle, \\ \pi^\dagger|n\rangle &= -\frac{i\hbar}{l_B}\sqrt{2n}|n-1\rangle, \end{aligned} \tag{23a}$$

$$\begin{aligned} K_- : \pi|n\rangle &= \frac{i\hbar}{l_B}\sqrt{2n}|n-1\rangle, \\ \pi^\dagger|n\rangle &= -\frac{i\hbar}{l_B}\sqrt{2(n+1)}|n+1\rangle. \end{aligned} \tag{23b}$$

The Hamiltonian of the monolayer-like band, Eq. (11a), describes two-dimensional Dirac-like fermions with a mass.

Although the entire spectrum of Landau levels can be found analytically for the monolayer block, for our purposes it suffices to consider only the zeroth LLs in $K_\pm$ valleys:

$$\Psi_{0^{\rm m}_+} = \begin{pmatrix} 0 \\ |0\rangle \end{pmatrix}, \quad E_{0^{\rm m}_+} = \delta - \frac{1}{2}\gamma_5 + \Delta_2, \tag{24a}$$

$$\Psi_{0^{\rm m}_-} = \begin{pmatrix} |0\rangle \\ 0 \end{pmatrix}, \quad E_{0^{\rm m}_-} = -\frac{1}{2}\gamma_2 + \Delta_2. \tag{24b}$$

Therefore, the zeroth LL in the monolayer sector is valley split, with the energy difference given by $\Delta^{\rm m}_\pm = E_{0^{\rm m}_+} - E_{0^{\rm m}_-} = \delta - \gamma_5/2 + \gamma_2/2 \approx 7$meV (where we used tight-binding parameters listed in Fig. 1). This situation should be contrasted with monolayer and bilayer graphene, where LLs are valley degenerate, at least at the single-particle level.[1]

Finding low-lying LLs in the bilayer block is more challenging. In general, the trigonal warping described by the first term in (14) does not allow us to solve for the LL spectrum analytically, as it breaks rotational symmetry and admixes arbitrarily high LLs. However, it turns out that trigonal warping gives relatively small corrections to LL energies, at least when the magnetic field is not too small.[28] Therefore, one can find the LL spectrum in the bilayer block neglecting trigonal warping, which gives

$$\Psi_{0^{\rm b}_+} = \begin{pmatrix} 0 \\ |0\rangle \end{pmatrix}, \quad E_{0^{\rm b}_+} = -2\Delta_2, \tag{25a}$$

$$\Psi_{1^{\rm b}_+} = \begin{pmatrix} 0 \\ |1\rangle \end{pmatrix}, \quad E_{1^{\rm b}_+} = -2\Delta_2 + \zeta\left(\frac{\gamma_5}{2} + \delta + \Delta_2\right), \tag{25b}$$

$$\Psi_{0^{\rm b}_-} = \begin{pmatrix} |0\rangle \\ 0 \end{pmatrix}, \quad E_{0^{\rm b}_-} = \frac{\gamma_2}{2} + \Delta_2, \tag{25c}$$

$$\Psi_{1^{\rm b}_-} = \begin{pmatrix} |1\rangle \\ 0 \end{pmatrix}, \quad E_{1^{\rm b}_-} = \frac{\gamma_2}{2} + \Delta_2 + \zeta(\delta - 2\Delta_2), \tag{25d}$$

where $\omega_c = eB/m = \sqrt{2}eBv^2/\gamma_1$ is the cyclotron frequency, and $\zeta = \hbar\omega_c/(\sqrt{2}\gamma_1)$ is a dimensionless parameter proportional to the magnetic field ($\zeta \approx 0.02$ for $B = 5$ T) that controls splitting between two LLs in the same valley. The intervalley splitting, approximately given by $\gamma_2/2 + 3\Delta_2$, is of the order of 10 meV; it is very sensitive to the value of Δ_2, since it enters with a factor of 3. Below we will see that even relatively small variations of Δ_2 can completely change the pattern of LL crossings at small negative filling factors. Also, notice that the intervalley splitting is much larger than the intravalley splitting: The latter is proportional to ζ and is of the order 1 meV at $B = 5$ T.

B. Landau levels at high bias

We now proceed with the analysis of the LL spectrum at a nonzero bias. As bias admixes the monolayer-like and bilayer-like blocks and trigonal warping becomes important, an approximate analytical treatment is no longer possible. Therefore, we find the LL spectrum and wave functions numerically.

If we fix the guiding center position at some value, our Hamiltonian can be viewed as an infinite matrix. It is easily written in the basis of nonrelativistic LL orbitals $|n\rangle$, using matrix elements of $\pi, \pi^\dagger$ operators from Eq. (23). We truncate this infinite matrix, restricting the Hilbert space to LL orbitals with indices $n \leqslant \Lambda$. Finally, the problem of finding the LL spectrum reduces to diagonalizing a matrix in which each element of the 6×6 Hamiltonian, Eq. (10), is replaced by a matrix of dimensions $\Lambda \times \Lambda$. Momentum operators are replaced by matrices corresponding to raising and lowering operators according to Eq. (23) with the cutoff Λ. All other nonzero elements γ_i are replaced by $\gamma_i \mathbb{1}_{\Lambda\times\Lambda}$.

One subtlety associated with this procedure is due to the fact that the cutoff imposed on the ladder operators gives rise to new unphysical eigenvalues.[30] Such unphysical eigenvalues have to be identified and removed. We do this by using the fact that although these "false" Landau levels have low energy, their wave functions are dominated by Landau level orbitals with large indices (near cutoff Λ). We have found that cutoff $\Lambda \gtrsim 30$ is sufficient to faithfully represent the evolution of LLs in the vicinity of the neutrality point with magnetic field and bias. All simulations presented in this paper are done with $\Lambda = 50$.

The evolution of LLs with magnetic field at zero bias is shown in Fig. 4(a). The zeroth LLs in the bilayer and monolayer block can be easily identified in this picture because they disperse very weakly with magnetic field. These results are consistent with Ref. 28; however, notice that we have chosen a different set of tight-binding parameters extracted from experiment,[5] which leads to visible differences in the LL spectrum.

The Landau level spectrum as a function of bias for fixed values of magnetic field $B = 5$ T and $B = 10$ T, illustrated in Figs. 4(b) and 4(c), reveals a very complex pattern of crossings. At smaller field $B = 5$ T and large bias $\Delta \gtrsim 0.15$ eV, both the dispersion and degeneracy of LLs changes: In particular, there are threefold-degenerate groups which are associated with the new emergent Dirac points in the band structure. In addition, there is a singly degenerate zeroth LL that originates from the central Dirac point in each valley. The dispersion of new zeroth LLs is determined by the dependence of the Dirac mass on the bias (see Fig. 3).

It should be noted that the threefold degeneracy of a subset of DPs gives rise to the threefold-degenerate groups of LLs only when the magnetic field is not too strong. This means that the inverse magnetic length must be smaller than the distance between the DPs in the BZ. Considering $\Delta_1 \gg 0.04$ eV and using the approximate expressions for the DP positions obtained in the previous section, we write this condition as $\hbar/l_B \ll \Delta_1/v_0$. Thus, threefold-degenerate groups of LLs are most easily observable at smaller fields.

Experimentally, the degeneracy of certain LLs at high bias (and relatively small field) will manifest itself in an anomalous quantum Hall sequence. Some of the steps will be characterized by a jump of Hall conductivity by $3e^2/h$ (when a threefold-degenerate LL is filled), while others will correspond to a jump of e^2/h (when a singly degenerate LL is filled). Here we assumed that the spin degeneracy is lifted by the Zeeman interaction. In experiment, such an anomalous quantum Hall sequence will signal the formation of new DPs.

C. Anticrossings and the role of γ_3

As we discussed above, bias gives rise to threefold-degenerate groups of LLs, which is in full agreement with the

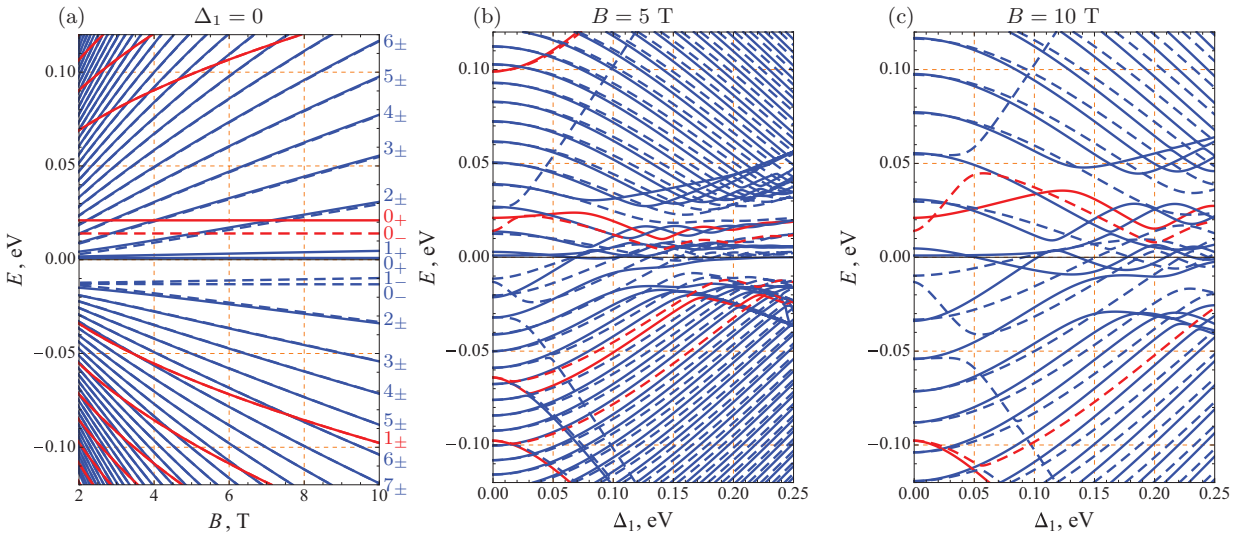

FIG. 4. (Color online) Landau level spectrum as a function of magnetic field and bias. Plot (a) shows LL spectrum as a function of magnetic field $B = 2 \ldots 10$ T at zero displacement field, $\Delta_1 = 0$, and $\Delta_2 = 0$. Landau levels from the monolayer-like and bilayer-like block are shown in red and blue color; solid (dashed) lines correspond to K_+ (K_-) valleys. LLs are labeled with their indices, e.g., blue 1_+, red 1_+ ($1^{\rm b}_+, 1^{\rm m}_+$ in the main text) stand for LL with index 1 from K_+ valley of bilayer and monolayer sector, respectively. Lifting of spin degeneracy by the Zeeman field is not shown, so that every LL is doubly degenerate. Neutrality point is located between blue 0_+ and blue 1_+ LLs. Plots (b) and (c) show Landau levels at $B = 5$ T and $B = 10$ T as a function of displacement field. Red (blue) color is used to indicate LLs which belong to monolayer (bilayer) sector at $\Delta_1 = 0$.

emergence of low-energy DPs in the band structure. Another notable feature of a LL pattern, which is visible in Figs. 4(b) and 4(c), is that LLs from the monolayer-like sector move away from the neutrality point as the bias is increased. This fact can also be understood using intuition developed about the band structure evolution under the bias: Hybridization and floating away of monolayer-like bands [see Figs. 2(a) and 2(b)] corresponds to monolayer-like LLs moving away and exhibiting avoided crossings with bilayer-like LLs.

Interestingly, it is the tight-binding parameter γ_3 that controls the behavior of the aforementioned avoided crossings. For example, let us zoom in to part of the LL spectrum corresponding to negative filling factors of order $\nu \approx -20$. We note that such filling factors are easily accessible in the experiment.[5] Figure 5 illustrates the pattern of avoided crossings for moderate bias $\Delta_1 = 0$–0.17 eV and two different values of γ_3: the one which is used in all simulations throughout this paper [$\gamma_3 = 0.39$ eV, Fig. 5(a)] and a twice larger value [$\gamma_3 = 0.78$ eV, Fig. 5(b)].

In Fig. 5(b), corresponding to the larger value of γ_3, the crossing pattern changes due to a slightly different order of LLs at zero bias. More noteworthy is the pronounced enhancement of gaps at anticrossings. Due to this enhancement, one can identify the clear pattern in Fig. 5(b): Avoided crossings occur between a given LL originating from monolayer-like band and every *third* bilayer-like LL. This pattern can be easily explained using the effect of trigonal warping on the LL wave functions. If, without a trigonal warping term, a given LL contains orbital $|i\rangle$ in its wave function, a nonzero trigonal warping admixes orbitals $|i \pm 3\rangle, |i \pm 6\rangle, \ldots$, with progressively smaller coefficients. It is this admixture that underlies the avoided crossings; thus, it is natural that stronger trigonal warping enhances the gaps at anticrossings.

As an example, let us consider LL $1^{\rm m}_+$ in the monolayer-like block (the labeling scheme of the LLs is introduced in the caption of Fig. 4). From Fig. 5 we see that it exhibits a pronounced anticrossing with the $8^{\rm b}_+$ bilayer-like LL, and also with the $11^{\rm b}_+$ LL for larger γ_3. In the absence of trigonal warping, the wave function of the $1^{\rm m}_+$ LL at $\Delta_1 = 0$ consists of a combination of $|0\rangle$ and $|1\rangle$ orbitals on $A_1 - A_3$ and $B_1 - B_3$ sublattices, respectively [see Eq. (9)]. The wave function of the $8^{\rm b}_+$ LL is dominated by $|6\rangle$ and $|8\rangle$ orbitals on

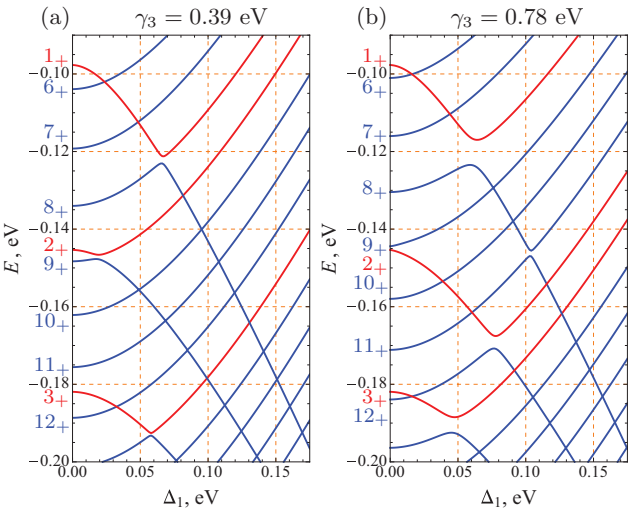

FIG. 5. (Color online) Influence of the value of γ_3 on the pattern of avoided crossings between monolayer-like and bilayer-like LL. Magnetic field is $B = 10$ T. For clarity, only LLs in the K_+ valley are shown. Plot (a) is for $\gamma_3 = 0.39$ eV used in this paper, whereas plot (b) is for twice larger value of γ_3. Labeling scheme of LLs is explained in the caption of Fig. 4.

a symmetric combination of $A_{1,3}$ sublattices and the B_2 sublattice. Nonzero trigonal warping changes the wave functions, admixing substantial components of $|0\rangle,|3\rangle,|9\rangle,\ldots$ orbitals to the $|6\rangle$ orbital on A_1+A_3 sublattice. Finally, nonzero Δ_1 breaks inversion symmetry, and initially orthogonal symmetric and antisymmetric combination of $A_{1,3}$ sublattices evolve to have nonvanishing overlap. This gives rise to the anticrossings observed in Fig. 5.

The observed sensitivity of the pattern of avoided crossings can be potentially used to fix the value of the tight-binding parameter γ_3. However, in order to do this, the other tight-binding parameters have to be refined. Below we discuss how information about them can be extracted from the LL crossings at small filling factors and a smaller bias.

D. Pattern of Landau level crossings at smaller bias and its sensitivity to tight-binding parameters

Having discussed the behavior of LLs at high bias and (or) large filling factors, we concentrate on the regime of small bias, when the new Dirac points have not formed yet. To better understand the complicated pattern of LL crossings that arises in this regime, we zoom in on the region $\Delta_1 \leqslant 0.1$ eV, and concentrate only on several low-lying LLs [see Fig. 6(a)].

Interestingly, the bias *completely* lifts the degeneracies of all LLs. Therefore, we expect that in biased bilayer graphene all quantum Hall plateaus will be spaced by e^2/h. Notice that this goes against intuition acquired from the studies of monolayer and bilayer graphene,[1] where in the absence of interactions Landau levels remain valley degenerate.

Landau levels undergo a series of crossings, as illustrated in Fig. 6(a). In particular, level $0^{\rm b}_-$ moves down, crossing weakly split $2^{\rm b}_\pm$ LLs at $\Delta_1 \approx 0.03$ eV. The energy of level $1^{\rm b}_-$ increases with bias, such that it crosses level $1^{\rm b}_+$ at $\Delta_1 \approx 0.07$ eV. Furthermore, levels $0^{\rm b}_+$ and $1^{\rm b}_+$ cross at $\Delta_1 \approx 0.05$ eV as the $1^{\rm b}_+$ level slowly moves down and the $0^{\rm b}_+$ level is essentially nondispersive. Finally, monolayer-like levels $0^{\rm m}_-$ and $0^{\rm m}_+$ both float up and cross at small bias $\Delta_1 \approx 0.015$ eV. They also cross the $2^{\rm b}_\pm$ LLs which move down.

As we emphasized above, although qualitatively the band structure of trilayer graphene is rather well understood at this point, not all parameters in the tight-binding model are precisely known. The complex LL crossing pattern described above is very sensitive to the choice of tight-binding parameters, and may provide a valuable tool for fixing their values. We illustrate this by exploring how the LL crossing pattern changes when parameter Δ_2 is varied. Such a parameter is allowed by symmetry, but has not been taken into account previously.

The LL crossing pattern for $\Delta_2 = 3$ meV and $\Delta_2 = 7$ meV is illustrated in Figs. 6(b) and 6(c). It is evident that the crossing between $1^{\rm b}_-$ and $1^{\rm b}_+$ is significantly shifted even by small $\Delta_2 = 3$ meV; so is the crossing between the monolayer-like $0^{\rm m}_+$ LL and $2^{\rm b}_\pm$ levels.

As Δ_2 is increased further [see Fig. 6(c)], new crossings appear; in particular, a pair $0^{\rm b}_+, 1^{\rm b}_+$ swaps positions with the pair $0^{\rm b}_-, 1^{\rm b}_-$ at zero bias [as expected from Eq. (25)]. This leads to new crossings between the $0^{\rm b}_-$ and $0^{\rm b}_+, 1^{\rm b}_+$ levels at a small bias, $\Delta_1 \approx 0.01$ eV. Also, the $0^{\rm m}_+$ LL moves above $2_\pm$ levels, such that crossings between them disappear. We see that even small variations of parameter Δ_2 can change the pattern of LL crossings. Similarly, the positions of different crossings are sensitive to the values of $\gamma_2, \gamma_5, \delta$, although in a more subtle manner.

As we pointed out, nonzero Δ_2 can be present among other tight-binding parameters. Moreover, if one accounts for the effect of the electric field self-consistently, in addition to renormalization of Δ_1 (corresponding to screening), parameter Δ_2 changes as well. We found that the typical value of Δ_2 obtained from such self-consistent procedure is 2 meV at the charge neutrality point.[31] We also performed numerical

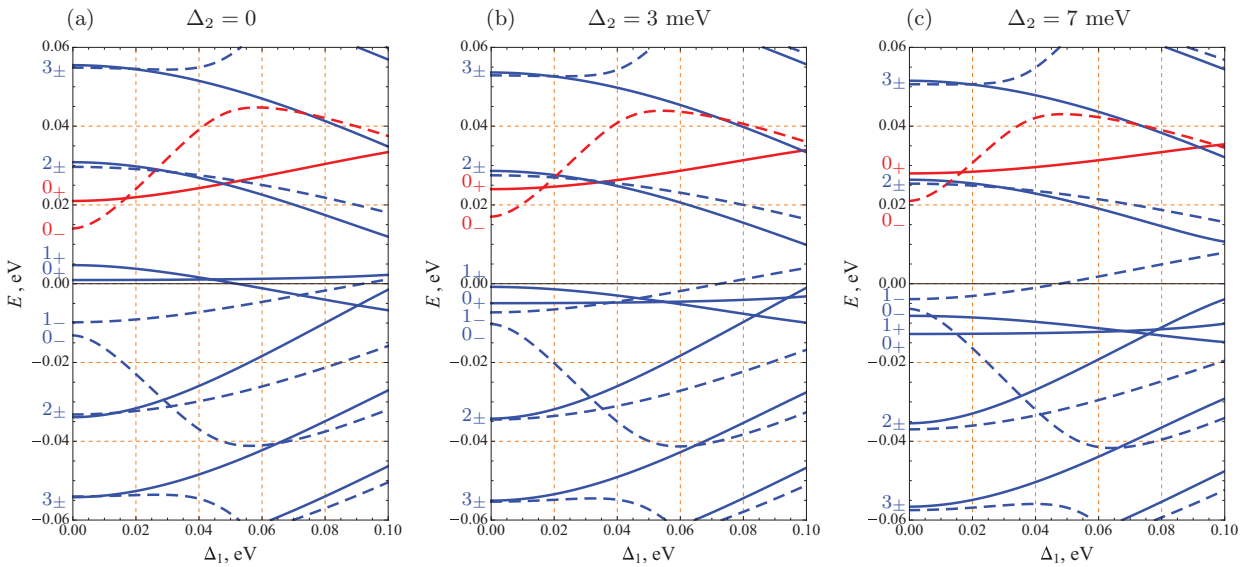

FIG. 6. (Color online) Landau levels as a function of displacement field for different values of Δ_2. Magnetic field $B = 10$ T. Plot (a) uses zero value of Δ_2; for plots (b) and (c) $\Delta_2 = 3$ meV and $\Delta_2 = 7$ meV, respectively. Value of $\Delta_2 = 7$ meV is sufficient to switch the order of blue $(1,0)_-$ and blue $(1,0)_+$ LLs from bilayer sector.

simulations for the case when a magnetic field is present (the detailed procedure will be described elsewhere). We found that the self-consistent value of Δ_2 in the presence of a magnetic field can be enhanced compared to the case when $B = 0$, due to discreteness of the LLs. For example, from Eqs. (25a) and (25b) one can see that at zero bias wave functions of bilayer-like $0^{\rm b}_{+}$ and $1^{\rm b}_{+}$, the LLs are localized on the middle layer. Consequently, by emptying these LLs one can create an excess positive charge on the middle layer, thus generating positive nonzero Δ_2 that can be as large as 4 meV.[31]

V. DISCUSSION AND OUTLOOK

In summary, we have studied the electronic properties of the ABA-stacked trilayer graphene in the perpendicular electric field. We found that the hybridization of the monolayer-like and bilayer-like bands leads to an opening of a small ($\lesssim$10 meV) band gap at experimentally achievable values of bias $\Delta_1 \lesssim 0.25$ eV. At bias $\Delta_1 \gtrsim 0.1$ eV, a new set of Dirac points appears in each valley, which includes one central DP, and six off-center DPs. Masses of the emergent Dirac fermions are tunable by bias, and, interestingly, some of the masses vanish at a bias which for our choice of tight-binding parameters corresponds to $\Delta_1^* \approx 0.185$ eV. Therefore, the band gap depends on the bias in a nonmonotonic manner and closes at the bias Δ_1^*. This behavior should be contrasted with bilayer graphene,[2–4] where the band gap grows monotonically as a function of bias, and can become very large, of the order of 0.25 eV.[4]

We have also studied the spectrum of LLs, finding that at bias $\Delta_1 \gtrsim 0.1$ eV the band structure transformation gives rise to new threefold-degenerate groups of LLs. The evolution of low-lying LLs from the unbiased case, where the spectrum consists of LLs in the monolayer and bilayer sectors, to the degenerate groups of LLs at higher bias is accompanied by multiple level crossings. Experimentally, these LL crossings will give rise to phase transitions between quantum Hall states as a function of bias. We have also shown that the pattern of crossings depends strongly on the values of certain tight-binding parameters, such as Δ_2 and γ_3. Studying the phase transitions in the QHE regime experimentally should enable the precise determination of these parameters.

Our results show that single-particle splittings between LLs in the biased trilayer are sizable, of the order of a few meV, and exceed the Zeeman energy of 1 meV at a typical magnetic field of $B = 10$ T. This is expected to play an important role in the analysis of quantum Hall ferromagnetism in trilayer graphene,[32–34] which will be the subject of a subsequent publication.[31] Here we just note that we found that, owing to the small LL spacing, the effective Coulomb interactions are strongly screened,[31] similar to the case of bilayer graphene[35] and, as a result, the Coulomb energy scale becomes comparable to typical single-particle energy splitting. This situation is quite different from the case of monolayer graphene, where single-particle splittings of LLs are much smaller than the interaction energy.[36–39]

Our study reveals the unique tunability of Landau levels in trilayer graphene: Bias controls their energies, wave functions, and degeneracies. We speculate that this may enable the exploration of interesting interaction-induced phenomena in the QHE regime. First, the threefold degeneracy of LLs at higher bias may allow one to study quantum Hall ferromagnetism, skyrmions, and fractional quantum Hall states with $SU(3)$ symmetry. Second, the bands in trilayer graphene are strongly trigonally warped, which provides an opportunity to study the effect of anisotropic band structure on quantum Hall ferromagnetism and fractional QHE.[40] Third, Landau level wave functions involve a superposition of different nonrelativistic LL orbitals with weights tunable by bias. Therefore the LL form factors are tunable, which may allow one to realize new effective interaction regimes, stabilize desired fractional quantum Hall states, and drive phase transitions between them.[20,21]

We believe that the phenomena discussed above can be experimentally observed in the near future. We note that the observation of effects associated with the emergent DPs is possible when disorder broadening is smaller than the energy scale over which effective description in terms of DPs is valid. Figure 2 indicates that the latter energy scale is of the order of 20 meV, which is much larger than the disorder broadening achievable in trilayer graphene on hexagonal boron nitride.[5,41] Therefore, new DPs should be observable in currently available samples.

Finally, we note that very recently multiple phase transitions between different quantum Hall states in biased trilayer graphene have been reported.[42] It is possible that these phase transitions can be understood in terms of single-particle LL spectrum evolution described in our paper.

Note added. We recently became aware of work by Morimoto and Koshino[43] in which new bias-induced Dirac points in trilayer graphene were also predicted. Recently ABA graphene subject to a large displacement field (several volts per nanometer) has been studied experimentally by K. Zou *et al.*[44] Such fields should be sufficient to study phenomena predicted in our work.

ACKNOWLEDGMENTS

We thank Pablo Jarillo-Herrero, Leonardo Campos, and Thiti Taychatanapat for attracting our attention to the problem of biased trilayer graphene, and for many helpful discussions.

[1] A. H. Castro Neto, F. Guinea, N. M. R. Peres, K. S. Novoselov, and A. K. Geim, Rev. Mod. Phys. **81**, 109 (2009).

[2] E. V. Castro, K. S. Novoselov, S. V. Morozov, N. M. R. Peres, J. M. B. Lopes dos Santos, J. Nilsson, F. Guinea, A. K. Geim, and A. H. Castro Neto, Phys. Rev. Lett. **99**, 216802 (2007).

[3] J. B. Oostinga, H. B. Heersche, X. Liu, A. F. Morpurgo, and L. M. K. Vandersypen, Nat. Mater. **7**, 151 (2008).

[4] Y. Zhang, T.-T. Tang, C. Girit, Z. Hao, M. C. Martin, A. Zettl, M. F. Crommie, Y. R. Shen, and F. Wang, Nature (London) **459**, 820 (2009).

[5]T. Taychatanapat, K. Watanabe, T. Taniguchi, and P. Jarillo-Herrero, Nat. Phys. **7**, 621 (2011).
[6]W. Bao, L. Jing, J. Velasco, Y. Lee, G. Liu, D. Tran, B. Standley, M. Aykol, S. B. Cronin, D. Smirnov, M. Koshino, E. McCann, M. Bockrath, and C. N. Lau, Nat. Phys. **7**, 948 (2011).
[7]C. H. Lui, Z. Li, K. F. Mak, E. Cappelluti, and T. F. Heinz, Nat. Phys. **7**, 944 (2011).
[8]A. Kumar, W. Escoffier, J. M. Poumirol, C. Faugeras, D. P. Arovas, M. M. Fogler, F. Guinea, S. Roche, M. Goiran, and B. Raquet, Phys. Rev. Lett. **107**, 126806 (2011).
[9]M. Koshino and E. McCann, Phys. Rev. B **79**, 125443 (2009).
[10]M. Koshino and E. McCann, Phys. Rev. B **80**, 165409 (2009).
[11]F. Zhang, B. Sahu, H. Min, and A. H. MacDonald, Phys. Rev. B **82**, 035409 (2010).
[12]M. Aoki and H. Amawashi, Solid State Commun. **142**, 123 (2007).
[13]M. Koshino and E. McCann, Phys. Rev. B **81**, 115315 (2010).
[14]M. Koshino and T. Ando, Phys. Rev. B **77**, 115313 (2008).
[15]M. Koshino and T. Ando, Phys. Rev. B **76**, 085425 (2007).
[16]A. A. Avetisyan, B. Partoens, and F. M. Peeters, Phys. Rev. B **80**, 195401 (2009); B. Partoens and F. M. Peeters, *ibid.* **75**, 193402 (2007); **74**, 075404 (2006).
[17]In this estimate we use values of tight-binding parameters from Ref. 5 and value $\varepsilon = 2$ for dielectric constant of ABA trilayer graphene.
[18]M. S. Dresselhaus and G. Dresselhaus, Adv. Phys. **51**, 1 (2002).
[19]S. H. R. Sena, J. M. Pereira, F. M. Peeters, and G. A. Farias, Phys. Rev. B **84**, 205448 (2011).
[20]Z. Papić, R. Thomale, and D. A. Abanin, Phys. Rev. Lett. **107**, 176602 (2011).
[21]Z. Papić, D. A. Abanin, Y. Barlas, and R. N. Bhatt, Phys. Rev. B **84**, 241306 (2011).
[22]C. L. Lu, C. P. Chang, Y. C. Huang, R. B. Chen, and M. L. Lin, Phys. Rev. B **73**, 144427 (2006).
[23]F. Guinea, A. H. Castro Neto, and N. M. R. Peres, Phys. Rev. B **73**, 245426 (2006).
[24]H. Min, B. Sahu, S. K. Banerjee, and A. H. MacDonald, Phys. Rev. B **75**, 155115 (2007).
[25]E. McCann and V. I. Fal'ko, Phys. Rev. Lett. **96**, 086805 (2006).
[26]It is also possible to obtain the velocity and mass of emergent Dirac fermions analytically (Ref. 43).
[27]M. Koshino, Phys. Rev. B **81**, 125304 (2010).
[28]M. Koshino and E. McCann, Phys. Rev. B **83**, 165443 (2011).
[29]S. Yuan, R. Roldán, and M. I. Katsnelson, Phys. Rev. B **84**, 125455 (2011).
[30]Extra Landau levels are introduced by cutoff imposed on ladder operators. Indeed, it is impossible to realize the algebra of raising and lowering operators $[a,a^\dagger] = 1$ with matrices of finite size: For any finite matrices A and B $\mathrm{tr}[A,B] = 0$. This fact manifest itself in the appearance of unphysical Landau levels which have to be removed.
[31]M. Serbyn and D. Abanin (unpublished).
[32]R. van Gelderen, L.-K. Lim, and C. M. Smith, Phys. Rev. B **84**, 155446 (2011).
[33]F. Zhang, D. Tilahun, and A. H. MacDonald, Phys. Rev. B **85**, 165139 (2012).
[34]Y. Sakurai and D. Yoshioka, Phys. Rev. B **85**, 045108 (2012).
[35]E. Gorbar, V. Gusynin, and V. Miransky, JETP Lett. **91**, 314 (2010).
[36]D. A. Abanin, P. A. Lee, and L. S. Levitov, Phys. Rev. Lett. **96**, 176803 (2006).
[37]K. Nomura and A. H. MacDonald, Phys. Rev. Lett. **96**, 256602 (2006).
[38]M. O. Goerbig, R. Moessner, and B. Douçot, Phys. Rev. B **74**, 161407 (2006).
[39]A. F. Young, C. R. Dean, L. Wang, H. Ren, P. Cadden-Zimansky, K. Watanabe, T. Taniguchi, J. Hone, K. L. Shepard, and P. Kim, Nat. Phys. **8**, 550 (2012).
[40]R.-Z. Qiu, F. D. M. Haldane, X. Wan, K. Yang, and S. Yi, Phys. Rev. B **85**, 115308 (2012).
[41]L. C. Campos, A. F. Young, K. Surakitbovorn, K. Watanabe, T. Taniguchi, and P. Jarillo-Herrero, Nat Commun. **3**, 1239 (2012).
[42]Y. Lee, J. Velasco, Jr., D. Tran, F. Zhang, W. Bao, L. Jing, K. Myhro, D. Smirnov, and C. N. Lau, arXiv:1210.6592.
[43]T. Morimoto and M. Koshino, Phys. Rev. B **87**, 085424 (2013).
[44]K. Zou, Fan Zhang, C. Clapp, A. H. MacDonald, and J. Zhu, Nano Lett. **13**, 369 (2013).